

Response to glassy disorder in coin on spread of quantum walker

Priya Ghosh, Kornikar Sen, Ujjwal Sen

Harish-Chandra Research Institute, HBNI, Chhatnag Road, Jhunsi, Allahabad 211 019, India

We analyze the response to incorporation of glassy disorder in the coin operation of a discrete-time quantum walk in one dimension. We find that the ballistic spread of the disorder-free quantum walker is inhibited by the insertion of disorder, for all the disorder distributions that we have chosen for our investigation, but remains faster than the dispersive spread of the classical random walker. While the inhibition to spread is common to all the distributions investigated, there are marked differences between the further behavior of the scalings for the different distributions. In particular, for disorder chosen from Haar-uniform and circular distributions, the response to weak disorder is weak, so that the scaling exponent falls off like a Gaussian against the disorder strength. However, for the spherical normal distribution and the two spherical Cauchy-Lorentz distributions, the response is strong even to weak disorder, and the fall-off is an exponential decay. Strong disorder universally leads to near, but faster than, the classical dispersive spread.

I. INTRODUCTION

In a classical random walk (CRW) on a line, the walker chooses to move left or right, depending on the result of a coin toss, and a pre-decided correlation between the two degrees of freedom. After a large number of steps, the position distribution of the walker is Gaussian and the corresponding spread, as quantified by the standard deviation, is proportional to the square root of the number of steps. A quantum version [1, 2] of the classical random walk has a standard deviation of the position distribution of the walker that is linear in the number of steps [3, 4]. Quantum walks (QWs) have since received a lot of attention [5–12], and have been applied to a plethora of scenarios, such as quantum algorithms [12–16], quantum memory [17, 18], and so on [3, 5, 19, 20]. They have also been used to model quantum state transfer [21–24]. QWs can - in the main - be classified into two categories, viz. discrete-[2, 25] and continuous-time [8, 20, 26] ones. Quantum walks have been experimentally realized in nuclear magnetic resonance systems, photons in waveguides, trapped atoms, synthetic gauge fields in a three-dimensional lattice, Fibonacci fibers, superconducting qubits, etc. [27–33].

Quantum walks have been discussed on different types of graphs such as Cayley graphs, percolation graphs, glued trees graphs, cyclic graphs, etc. for discrete [34–37] as well as continuous [38–41] quantum walks. Topological behavior (topological invariants and topological phases) of quantum walks has also been illustrated, both theoretically [7, 42–44] and experimentally [45–49]. Quantum walks in presence of decoherence and jumps were also studied [50–53]. It has been used as a powerful tool in simulations of physical processes such as photosynthesis, breakdown of electric-field-driven systems, and so on [54–56].

Imperfections are ubiquitous in physical systems, and it is important to consider their effects in physical phenomena and devices. While imperfections in the form of disorder or noise are typically expected to reduce the visibility in the order parameter of a phenomenon and the efficiency of a device, it has surprisingly been also found to increase visibilities and efficiencies in certain cases [57–63]. It is therefore natural to consider the effects of disorder insertion in quantum walks [64–98]. It has been seen that the spread of a quan-

tum walker can get reduced in the presence of noise. Imperfections have been considered in the quantum coin [64–69, 74, 77, 78, 82, 85, 88, 95] as well as in the step length of the walker [93, 96]. At least three types of disorder have been identified and imposed on the quantum coin - static (position dependent coin) [66, 69, 77, 78, 88], dynamic/temporal (time dependent coin) [64, 65, 67, 68, 82, 85, 95], fluctuating disorder (coin as a function of both time and position) [74].

In this work, we focus on one-dimensional (1D) discrete-time quantum walks (DQWs). We explore the spreading of the quantum walker in presence of glassy or quenched disorder in the coin operator. We find that the disorder-averaged spread of the position distribution of the quantum walker is slower than the case when there is no disorder. We quantify the spread by using the position distribution's standard deviation. While the inhibition is common to all the distributions considered, there are clear differences in the behaviors of the scaling exponents of the spread for different distributions. In particular, the fall-off, from the ballistic spread in the disorder-free case, for increasing disorder that is still weak, can be Gaussian or an exponential decay. For strong disorder, the spread is near-dispersive, but universally remains super-dispersive. The classical random walker has a dispersive spread. The disorder distributions considered are Haar-uniform with a finite cut-off, spherical normal (von Mises - Fisher), circular, and two spherical Cauchy-Lorentz distributions. We find that the fall-offs for weak disorder are similar for uniform and spherical Cauchy-Lorentz distributions, for which the decay is exponential. For the remaining two, the fall-off is slower and Gaussian.

The structure of the remaining parts of the paper is as follows. In Sec. II, we briefly recapitulate some general aspects of 1D DQWs. Sec. III consists of a concise discussion on quenched disorders in general, and the model of the coin's disorder that we use. We then briefly discuss, in Sec. IV, the different types of probability distributions on a sphere that we use for prototyping the disorder distribution in the coin operator. The momentum representation is considered in Sec. V A, the analytical considerations in which help in the numerical analysis beyond. The scaling analysis is presented in the remaining portion of Sec. V. A conclusion is given in Sec. VI.

II. ABOUT QUANTUM WALK

The 1D discrete-time CRW is a stochastic process which represents the path of a “drunk” walker. It consists of taking a step to the left or right of the current position, with the direction being decided by another degree of freedom, a “classical coin”, and this process tossing the coin and moving a step according to the result of the toss is repeated many times. Brownian motion of gas or liquid molecules has been modelled by CRWs [99, 100].

In the quantum analogue of discrete-time CRWs, both the walker and the coin are described as quantum systems, and they are typically quantum coherent [101–107] and entangled [108–111] at almost all instants. We denote the Hilbert space of the coin by \mathcal{H}_c , with the elements of the computational basis, $\{|0\rangle, |1\rangle\}$, representing “head” and “tail” in a “coin toss”. As we will see, the coin toss in a quantum walk is “coherent” and not a measurement in the computational basis. The Hilbert space of the walker, on the other hand, is denoted by \mathcal{H}_w , with the set of positions of the walker in different steps, $\{|i\rangle : i \in \mathcal{Z}\}$, spanning it, where \mathcal{Z} is the set of integers. Although the dimension of \mathcal{H}_w is \aleph_0 , after t steps taken by the walker, the state of \mathcal{H}_w , written in the position basis will have nonzero coefficients only for the basis elements $|i\rangle$, with $i \in [-t, t] \cap \mathcal{Z}$, if the initial position is at $|0\rangle$. The Hilbert space of the total system consisting of the walker and the coin is $\mathcal{H}_{tot} = \mathcal{H}_c \otimes \mathcal{H}_w$.

In DQWs, the walker’s direction for each movement will be decided coherently by the state of the coin at that step. We assume that if the coin is in the state, $|0\rangle, |1\rangle$, in any particular step, then the walker will move one step towards the right (left). The tossing of the coin is represented using the coin operator, C , which is a unitary gate acting on the Hilbert space \mathcal{H}_c , whereas the evolution of the walker is achieved by the conditional shift operator, \tilde{S} , on \mathcal{H}_{tot} , given by

$$\tilde{S} = \sum_{i=-t}^t |0\rangle\langle 0| \otimes |i+1\rangle\langle i| + |1\rangle\langle 1| \otimes |i-1\rangle\langle i|. \quad (1)$$

Hence if the initial state of the composite system is $|\psi_{tot}\rangle$, then the state after one iteration, i.e., after taking one step is given by $|\psi'_{tot}\rangle = \tilde{S}(C \otimes I)|\psi_{tot}\rangle$. Note that both CRWs and DQWs have the parity property, in that after an even (odd) number of steps, the probability of finding the walker at odd (even) displacements is zero. But in the quantum case, the variance of the position distribution of the walker varies quadratically with time, i.e., with the number of steps.

In DQWs, one typically uses the Hadamard gate,

$$H = \frac{1}{\sqrt{2}} \begin{pmatrix} 1 & 1 \\ 1 & -1 \end{pmatrix}$$

for the coin tossing operator, C , and in such case, the walk may be referred to as the “Hadamard walk”. The position distribution can be asymmetric, with symmetric ones obtained by using the initial state of the coin as

$$|\psi_c^{in}\rangle = (|0\rangle + i|1\rangle) / \sqrt{2},$$

or by using the operator,

$$Y = \frac{1}{\sqrt{2}} \begin{pmatrix} 1 & i \\ i & 1 \end{pmatrix},$$

as the coin operation, C . In this work, we consider the initial states of the quantum coin and the walker as $|\psi_c^{in}\rangle$ and $|0\rangle$ respectively. We set

$$|\psi_{tot}^{in}\rangle = |\psi_c^{in}\rangle \otimes |0\rangle.$$

The coin operator will be chosen as one that is Hadamard “on average, but with a spread”. The meaning of this statement will be made precise below.

III. DISORDER IN COIN OPERATION

We wish to examine the effect of incorporation of a “glassy” disorder on the spreading of the quantum walker. The disorder is called “glassy”, as the typical equilibration time of the disorder is assumed to be several orders of magnitude higher than the typical observation times that we are interested in. This type of disorder is also called “quenched” disorder in the literature.

We introduce the disorder on the quantum coin in such a way that instead of transforming the state $|0\rangle (|1\rangle)$ on $(|0\rangle + |1\rangle) / \sqrt{2}$ ($(|0\rangle - |1\rangle) / \sqrt{2}$), the coin operator projects $|0\rangle (|1\rangle)$ to the state, $|\xi(\theta, \phi)\rangle (|\xi^\perp(\theta, \phi)\rangle)$, on the surface of the Bloch sphere. The states $|\xi(\theta, \phi)\rangle$ and $|\xi^\perp(\theta, \phi)\rangle$ can be described using the spherical polar angles, θ, ϕ . The disorder chooses the values of (θ, ϕ) by following certain probability distributions. We will discuss later about the choice of the probability distribution. We name such a coin operator as a *biased* Hadamard gate. Such a gate is of course not strictly “biased”, unless $\phi \neq 0$, which, however, happens almost all the time.

As stated before, we wish to consider the effect of glassy disorder on the QW. More precisely, we wish to analyze the response to disorder insertion in the spread of the walker. At any particular step, the coin operator is chosen by randomly choosing the coin-operator parameters, θ, ϕ , from a pre-decided probability distribution. The choice at any particular step is made independently of the choice in any other step. We are interested in the spread of walker, as quantified by the standard deviation of the position distribution. For a given set of configurations of the disorder in a particular run, we calculate the spread, and then average over the disorder. This mode of averaging of a physical quantity *after* its evaluation, has been called “quenched” averaging. Let the state of the composite system, consisting of the walker and the coin, after t steps be $|\psi_{tot}^t\rangle$. Then the state of the walker after t steps is

$$\rho_t = \text{Tr}_c(|\psi_{tot}^t\rangle\langle\psi_{tot}^t|),$$

where Tr_c denotes the partial trace taken over the coin’s Hilbert space, \mathcal{H}_c . Then the variance of the position of the walker is given by

$$\sigma^2(\rho_t) = \sum_i \langle i | \rho_t^2 | i \rangle - \left(\sum_i \langle i | \rho_t | i \rangle \right)^2.$$

We denote the quenched averaged standard deviation after t steps as $\langle \sigma(t) \rangle$.

IV. CLASSIC PROBABILITY DISTRIBUTIONS ON SPHERE

For the situation that we are considering, when the coin is without any disorder, the coin operator is the Hadamard gate, which takes the σ_z eigenbasis onto the σ_x eigenbasis. In the disordered case, the target basis is $\{|\xi(\theta, \phi)\rangle, |\xi^\perp(\theta, \phi)\rangle\}$, with a certain distribution for the spherical polar coordinates, θ, ϕ . In a realistic case, we expect this target basis to be close to the σ_x eigenbasis and distributed symmetrically around it. We are therefore looking for probability distributions that are symmetrically distributed around $(\theta, \phi) = (\pi/2, 0)$ on the unit sphere, to define the state $|\xi(\theta, \phi)\rangle$. This automatically fixes the state $|\xi^\perp(\theta, \phi)\rangle$, except for a phase, which is arbitrarily chosen to be such that the biased Hadamard gate is $H(\theta, \phi)$ of Eq. (3).

We are mainly interested in the quenched-averaged dispersion, $\langle \sigma(t) \rangle$, of the disordered quantum walk. We want to study how $\langle \sigma(t) \rangle$ depends on the number of steps, t . In particular, we want to estimate the “scaling”, with the number of steps, of average dispersion of the disordered quantum walk, and its behavior with respect to the “strength” of the disorder. The meaning of the strength of a disorder will depend on the disorder distribution chosen, as we will see below. The scaling of the dispersion is defined as α , where

$$\langle \sigma(t) \rangle \propto t^\alpha. \quad (2)$$

It is known that $\alpha = 1$ in case of the ordered quantum walk, whereas in case of the classical random walk, it is 0.5. To find the value of α in a disordered quantum walk, we numerically evaluate $\langle \sigma(t) \rangle$ for different iterations, t , from 8 to 24, with intervals of 2, for each type of probability distribution of the disorder that we consider. These evaluations, obtained through log-log scaling plots, are correct up to two significant figures. We discuss now about the various distributions for disorder that we consider.

From now on, we will use the following notation. When a point in the 3D space is expressed using the Cartesian coordinate system, we will use “ c ” in the suffix of the vector, and when the coordinate system is spherical polar, we will use “ s ” in the suffix. For example, $(r, \theta, \phi)_s$ is the spherical polar representation of a point, whereas the corresponding Cartesian representation is $(x, y, z)_c$, where $x = r \sin \theta \cos \phi$, $y = r \sin \theta \sin \phi$ and $z = r \cos \theta$.

A. Uniform distribution

We begin with a distribution for which the points, $(1, \theta, \phi)_s$, are uniformly distributed on the surface of a unit sphere (with center at the origin). As we have mentioned previously, we want a distribution that is symmetric about the point $(1, 0, 0)_c$, i.e., $(1, \pi/2, 0)_s$, and we will define a “cut-off” (range) of the Haar-uniform generation of the points on the curved surface,

so that a (possibly small) symmetric region around $(1, \pi/2, 0)_s$ is utilized. Consider a plane parallel to the $y - z$ plane cutting the surface of the sphere in two parts. Let us denote the distance of the plane from the point $(1, 0, 0)_c$ as r_U . This parameter, r_U , describes the range of the distribution and can vary within $[0, 2]$, as the radius of the Bloch sphere is unity. The random numbers $(1, \theta, \phi)_s$ are drawn from the surface of that part of the sphere which belongs to the positive x direction of the plane. Haar-uniform distribution on sphere can be constructed by uniform selection of $\cos \theta$ and ϕ within the range specified by range parameter r_U . Since the distribution is symmetric about the point $(1, 0, 0)_c$, whatever be the range, the direction of the mean of the distribution will always be $(1, 0, 0)_c$. In Fig. 1, we plot points chosen from the Haar-uniform distribution with different ranges, r_U , on a purple sphere. We plot 10^4 points for each value of r_U .

Later, we will evaluate scaling of the DQW with the disorder in its coin being chosen from different Haar-uniform distributions within the range $r_U \in [0, 2]$. We will employ r_U to quantify the strength of the disorder being used.

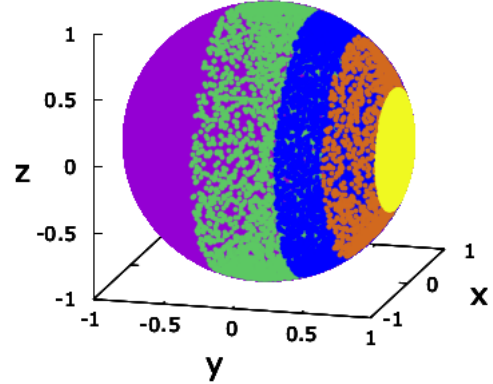


FIG. 1: Uniform distribution on a sphere. We exhibit here uniform distributions of points for different ranges, on a purple unit sphere, with the mean direction of the distribution being along $(1, 0, 0)_c$. The different color points, *viz.* yellow, orange, blue, and green are chosen from uniform distributions with ranges (r_U) 0.1, 0.4, 0.7, and 1.3 respectively. There are 10^4 points for each range. The uniform generations utilize the methods of Haar-uniform generation on a sphere. All quantities used are dimensionless.

B. Spherical normal distribution

Next we consider a “spherical normal” distribution, i.e., we want to choose the random biased Hadamard gates such that the (θ, ϕ) corresponding to the $|\xi(\theta, \phi)\rangle$, of the gates, are “spherical normally” distributed on the Bloch sphere, around the state $(|0\rangle + |1\rangle)/\sqrt{2}$. The von Mises - Fisher distribution (vMFD) has been interpreted as a normal distribution on a sphere [112]. It is described using two parameters, κ_N, μ_N ,

and the probability measure is

$$p(\theta, \phi) d\theta d\phi = A \exp(\kappa_N \mathbf{x}^T \cdot \boldsymbol{\mu}_N) \sin \theta d\theta d\phi,$$

where $\kappa_N \in [0, \infty)$ is called the concentration parameter and $\boldsymbol{\mu}_N \equiv (\mu_x, \mu_y, \mu_z)_c$ represents the mean direction. Here, $\mathbf{x} \equiv (\sin \theta \cos \phi, \sin \theta \sin \phi, \cos \theta)_c$ and A is the normalization constant. As one increases the value of κ_N , the distribution becomes more and more concentrated around the mean direction, $\boldsymbol{\mu}_N$. The vMFD becomes the uniform distribution for $\kappa_N \rightarrow 0$, whereas it leads to the ordered case for $\kappa_N \rightarrow \infty$.

Considering a mean direction along $(0, 0, 1)_c$, we get the simpler-looking distribution, given by

$$p(\theta) d\theta = \frac{\kappa_N}{2 \sinh \kappa_N} \exp(\kappa_N \cos \theta) \sin \theta d\theta,$$

$$p(\phi) d\phi = d\phi.$$

To take advantage of this simpler form, we choose random points (θ, ϕ) from this distribution which has mean at $(0, 0, 1)_c$, and then rotate those points to get a distribution with mean direction $(1, 0, 0)_c$.

In Fig. 2, we plot points $(1, \theta, \phi)_s$ chosen randomly from vMFs with $\boldsymbol{\mu}_N = (1, 0, 0)_c$ and varying κ_N . One can see in Fig. 2 that as the value of κ_N decreases, spreading of the distribution increases. Thus we can define the range or strength of the disorder as $r_N = \frac{1}{\sqrt{\kappa_N}}$, which is exactly equal to the standard deviation of the vMF distribution. The quenched averaged dispersion of the spread of the position of the quantum walker, when the disorder in the biased Hadamard gate is chosen from the vMF distribution, in Sec. V C.

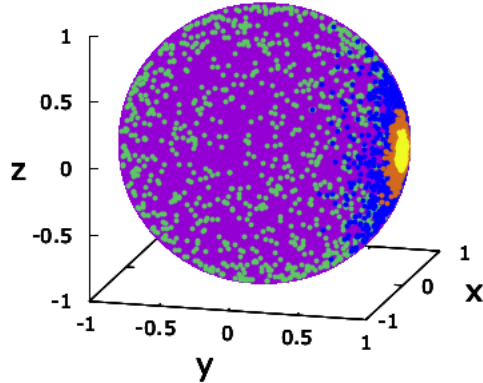


FIG. 2: Spherical normal distribution. We plot points on a purple unit sphere, randomly generated from von Mises - Fisher distributions, with mean direction as $(1, 0, 0)_c$ and different concentration parameters, κ_N . The different colors, *viz.* yellow, orange, blue, and green, denote points chosen from distributions with $\kappa_N = 500, 100, 10$, and 0.1 respectively. We have generated 10^3 points for each concentration value. All quantities used are dimensionless.

C. Circular distribution

Discrete probability distributions form an important category for studies of disorder incorporation in physical systems. If the disorder is being inserted in a scalar quantity, the discrete probability distribution that one would typically consider is one which takes the values $\pm r_D$, assuming that the intended mean is at zero. Arguably, the parallel in the case when we are required to scatter the distribution on a sphere, will be given by circles on the sphere, symmetrically around the intended mean direction. We note that when generalized in this way, the distribution is actually not discrete, but no discrete distribution will be rotationally symmetric about a mean direction.

Since we wish to have the mean direction as $(1, \pi/2, 0)_s$, these circles will be parallel to the $y - z$ plane. We name these as the circular distributions, and denote the radius of such a circle by $r_C \in [0, 1]$, so that its center is at $(\sqrt{1 - r_C^2}, 0, 0)_c$. We will use r_C to quantify the strength of a circular distribution. Fig. 3 portrays circular distributions for different values of r_C . In the succeeding section, this distribution will be among the ones that are used for disorder insertion in the coin operator.

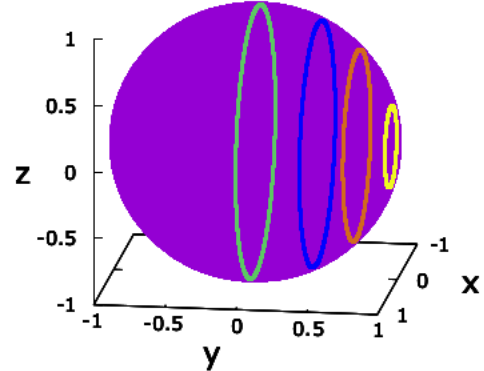


FIG. 3: Circular distribution on a sphere. We generate, and plot, points chosen from circular distributions on the unit sphere of different ranges, r_C . For each range, we generate 10^4 points. The different colors, *viz.* yellow, orange, blue, and green represent points drawn from distributions of ranges $0.3, 0.7, 0.9$, and 1 respectively. All quantities used are dimensionless.

D. Spherical Cauchy-Lorentz distributions

In studies about disorder insertion in system parameters on a flat parameter space, one often considers the Cauchy-Lorentz distribution, which, although has a profile similar to the Gaussian one, is starkly different from it, as the former does not have a finite mean and standard deviation, though a Cauchy mean value does exist. In the literature, there are at least two distributions that has been claimed to be generalizations to the sphere of the Cauchy-Lorentz distribution on a flat

parameter space.

1. Spherical Cauchy-Lorentz I

The probability measure of one of them is given by

$$p(\theta, \phi)d\theta d\phi = \frac{1}{2 \ln \delta} \frac{(\delta^2 - 1)}{(\delta^2 + 1) - (\delta^2 - 1)\mathbf{x}^T \cdot \boldsymbol{\mu}_1} \sin \theta d\theta d\phi.$$

It is dependent on the two parameters, δ and $\boldsymbol{\mu}_1$, acting respectively as a concentration parameter and the mean direction. The range of δ is $[0, \infty) \setminus \{1\}$. As $\delta \rightarrow 1$, the distribution becomes more and more uniform over the whole unit sphere [113]. The mean direction is $\boldsymbol{\mu}$ for $\delta > 1$, and $-\boldsymbol{\mu}$ for $\delta < 1$. The x - and y -components of the standard deviation vector are equal and has a supremum as $\delta \rightarrow 1$. The z -component is in general unequal to the other two components, but has a supremum at the same point.

To generate points from this distribution, we first assume that the direction of the mean is along z -axis, i.e. $\boldsymbol{\mu}_1 = (0, 0, 1)$. The measure for the distribution, therefore, becomes

$$p(\theta)d\theta = \frac{1}{2 \ln \delta} \frac{(\delta^2 - 1)}{(\delta^2 + 1) - (\delta^2 - 1)\cos \theta} \sin \theta d\theta,$$

$$p(\phi)d\phi = d\phi.$$

After generating points using this distribution, we rotate the points to get a distribution with mean along the x -axis. A few such distributions are exhibited in Fig. 4 for certain values of δ . It is visible from Fig. 4 that as δ decreases from a higher value towards 1 the distribution becomes less concentrated along the mean direction and more uniform over the sphere. But if δ become less than 1 the distribution will drop its uniform nature and will again start to get concentrated, but now around the direction opposite to that of $\boldsymbol{\mu}_1$. Thus how much the disorder can distort the actual property of the coin can be quantified using the parameter $r_{C1} = 1/\delta$.

2. Spherical Cauchy-Lorentz II

Another distribution on the unit sphere that has been considered as a generalization of the Cauchy-Lorentz distribution can be defined again using two parameters, *viz.* ρ and $\boldsymbol{\mu}_2$, and for which the probability measure is given by

$$p(\theta, \phi)d\theta d\phi = \frac{1}{4\pi} \frac{(1 - \rho^2)^2}{(1 + \rho^2 - 2\rho\boldsymbol{\mu}_2^T \cdot \mathbf{x})^2} \sin \theta d\theta d\phi,$$

where $\rho \in [0, 1)$ and $\boldsymbol{\mu}_2$ work as the concentration parameter and the direction of the mode of the distribution respectively. As ρ goes to zero, the distribution becomes uniform, and on the other hand, the distribution converges to a point distribution when ρ tends to 1 [114].

Again taking the direction of the mode along the z -axis, the measure for the distribution reduces to

$$p(\theta)d\theta = \frac{1}{4\pi} \frac{(1 - \rho^2)^2}{(1 + \rho^2 - 2\rho \cos \theta)^2} \sin \theta d\theta,$$

$$p(\phi)d\phi = d\phi.$$

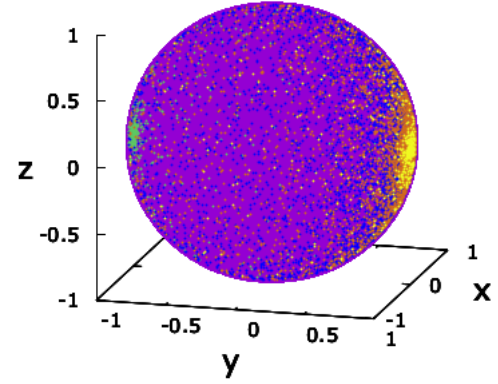


FIG. 4: Nature of Cauchy-Lorentz I distribution on a sphere. We sample 10^3 pairs of angles, (θ, ϕ) , from each of the Cauchy-Lorentz I distributions having $\delta = 10^4, 10^2, 10, 10^{-4}$. They are plotted on a unit purple sphere using yellow, orange, blue, and green colors respectively. All quantities used are dimensionless.

Generating points using this distribution, and then rotating the points appropriately, we can get the required distribution having mode along the x -axis. The variation of the pattern of the distribution can be seen in Fig. 5. As ρ tends to zero, the distribution becomes more and more uniform. Thus, we can quantify the strength of disorder using $r_{C2} = 1/\rho$.

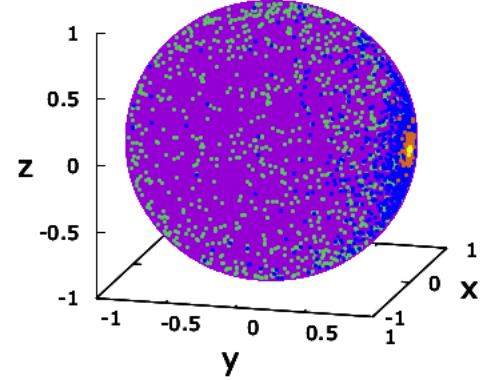


FIG. 5: Cauchy-Lorentz II distribution on a sphere. We generate, and plot, 10^3 points for every chosen ρ from the Cauchy-Lorentz II distribution on the purple unit sphere. The concentration parameter is chosen as 0.999, 0.98, 0.7, and 0.1, and represented using yellow, orange, blue, and green colored dots respectively. All quantities used are dimensionless.

The scalings of the quenched averaged dispersion of the quantum walk for both the spherical Cauchy-Lorentz distributions are analyzed in the succeeding section.

V. RESPONSE TO DISORDER

The scaling exponent of dispersion of an ordered Hadamard quantum walk is unity, being double of that for the classical random walker. But we will find, in this section, that in the presence of disorder in the coin operator, this ballistic spread in the quantum case becomes sub-ballistic, although remains super-diffusive, with the diffusive spread being reached by the classical random walker. While this qualitative feature remains unchanged for all the disorder distributions that we have considered, the actual scale exponents and their behavior with strength of the disorder differ significantly from one distribution to the other.

Here we estimate scalings of the dispersions of disordered quantum walks for each of the distributions discussed in the preceding section, for varying disorder strengths. After fixing a distribution of the disorder, we analyze the scaling exponent, α , of the quantum walker's spread. In particular, we look at its behavior as a function of the strength of the disorder. In each of these cases, we try to fit a curve, and estimate the curve parameters via the least-squares method. We also estimate the fitting error in each case. The method is briefly defined here for completeness. For a set of N data points, $(x_1, y_1), (x_2, y_2), \dots, (x_N, y_N)$, to which we fit the curve $y = y(x|a_1, a_2, \dots, a_M)$, involving M parameters, a_1, a_2, \dots, a_M , we set

$$\chi^2 = \sum_i \left[\frac{y_i - y(x_i|a_1, \dots, a_M)}{\sigma_i} \right]^2.$$

The quantity σ_i represents the standard deviation of the i^{th} data point. We assume that they are equal to each other in our analysis. The maximum-likelihood estimate of the fitting parameters are obtained by minimizing χ^2 . The corresponding error is given by $\sqrt{\sigma^2 \chi^2 / (N - M)}$, where σ is the common value of the σ_i .

We begin by going over to the momentum representation, which aids in the evaluation of the scaling exponents. Subsequently, we consider the different disorder distributions and their respective exponents.

A. Momentum representation

The amplitude of the quantum walker at the n^{th} position at time t can be written as

$$|\Psi(n, t)\rangle = \begin{pmatrix} \Psi_1(n, t) \\ \Psi_0(n, t) \end{pmatrix},$$

where $\Psi_1(n, t)$ and $\Psi_0(n, t)$ denote the amplitudes of the quantum walker at position n at time t , with the quantum coin being in $|1\rangle$ and $|0\rangle$ respectively. To move on to the next step, we have to first operate the biased Hadamard gate on the coin's space and then have to act the shift operator on the composite space. The coin operator, C , is now to be chosen as the biased Hadamard gate, given by

$$H(\theta, \phi) = \begin{pmatrix} \cos(\theta/2) & \sin(\theta/2) \\ \sin(\theta/2)e^{i\phi} & -\cos(\theta/2)e^{i\phi} \end{pmatrix}, \quad (3)$$

where θ and ϕ are randomly chosen parameters from the probability distribution of the disorder.

Since the shift operator moves the walker only one step towards to its left or right, the amplitude $|\Psi(n, t+1)\rangle$ will have contributions from $|\Psi(n-1, t)\rangle$ and $|\Psi(n+1, t)\rangle$ only. Hence the former can be expressed in terms of the latter in the following way (compare with [4]):

$$|\Psi(n, t+1)\rangle = M_-(\theta, \phi) |\Psi(n-1, t)\rangle + M_+(\theta, \phi) |\Psi(n+1, t)\rangle. \quad (4)$$

It can be seen that

$$M_-(\theta, \phi) = \begin{pmatrix} 0 & 0 \\ \sin(\theta/2)e^{i\phi} & -\cos(\theta/2)e^{i\phi} \end{pmatrix},$$

$$M_+(\theta, \phi) = \begin{pmatrix} \cos(\theta/2) & \sin(\theta/2) \\ 0 & 0 \end{pmatrix}.$$

Eq. (4) is the recursion relation for the quantum walk using the disordered Hadamard gate. The Fourier transform of $|\Psi(n, t)\rangle$ is

$$|\tilde{\Psi}(k, t)\rangle = \sum_{n=-\infty}^{+\infty} |\Psi(n, t)\rangle e^{ikn}.$$

Then using Eq. (4), we can write $|\tilde{\Psi}(k, t+1)\rangle$ in terms of $|\tilde{\Psi}(k, t)\rangle$ in the following manner:

$$|\tilde{\Psi}(k, t+1)\rangle = \sum_{n=-\infty}^{+\infty} (M_- |\Psi(n-1, t)\rangle + M_+ |\Psi(n+1, t)\rangle) e^{ikn},$$

$$\Rightarrow |\tilde{\Psi}(k, t+1)\rangle = (e^{ik} M_- + e^{-ik} M_+) |\tilde{\Psi}(k, t)\rangle$$

$$\Rightarrow |\tilde{\Psi}(k, t+1)\rangle = M_k(\theta, \phi) |\tilde{\Psi}(k, t)\rangle.$$

Here, $M_k(\theta, \phi)$ is given by

$$M_k(\theta, \phi) = \begin{pmatrix} e^{-ik} \cos(\theta/2) & e^{-ik} \sin(\theta/2) \\ e^{ik} \sin(\theta/2)e^{i\phi} & -e^{ik} \cos(\theta/2)e^{i\phi} \end{pmatrix}.$$

Therefore, by starting with the initial state $|\tilde{\Psi}(k, 0)\rangle$, if we take t steps, then the final momentum-space amplitude is given by

$$|\tilde{\Psi}(k, t)\rangle = M_k(\theta_t, \phi_t) M_k(\theta_{t-1}, \phi_{t-1}) \dots M_k(\theta_1, \phi_1) |\tilde{\Psi}(k, 0)\rangle.$$

In the noiseless scenario, i.e., in the case when there is no disorder, the above equation reduces to $|\tilde{\Psi}(k, t)\rangle = M_k^t(\pi/2, 0) |\tilde{\Psi}(k, 0)\rangle$. This final state, and the corresponding spread in position, can be obtained by using the spectral decomposition of $M_k(\pi/2, 0)$, and subsequently finding the inverse Fourier transform of $|\tilde{\Psi}(k, t)\rangle$. In the disordered case, however, $M_k(\theta, \phi)$ is different in each step.

B. Uniform disorder

We now consider the case of uniform disorder with a fixed range. Since the parameter space is not flat, one needs to consider the suitable Haar-uniform probability measure, as discussed in Sec. IV A. For a given strength, r_U , of the uniform disorder, we determine the standard deviation for each disorder configuration, and then find the standard deviation of the

walker's position distribution for that configuration. We subsequently average over the different disorder configurations, each of which is picked independently and at random from the uniform distribution on the sphere for the chosen range, r_U . Subsequently, we calculate the scaling exponent (see Eq. (2)) for the chosen r_U . We repeat the calculation to check for convergence by choosing a larger number of disorder configurations for the same r_U . We perform this arithmetic for several values of r_U , to understand the profile of the scaling exponent as a function of the disorder strength, r_U . In Fig 6, we plot the scaling exponent, α , versus the disorder strength, r_U . The profile matches well with an exponential function:

$$\alpha = a_U \exp(-b_U r_U) + c_U, \quad (5)$$

where the the parameter values are given by $a_U = 0.489 \pm 0.00240$, $b_U = 1.89 \pm 0.0275$, $c_U = 0.502 \pm 0.00199$, being obtained from a least-square fitting method, with the error being 0.00366. The numbers appearing after the \pm sign indicate the 95% confidence interval. All numerical data are correct to three significant figures. We observe that as a response to uniform disorder, the scaling exponent of dispersion of the quantum walker's position reduces quite quickly (from the unit scaling exponent of the ordered case) for small values of the disorder strength. However, it never reaches the value 0.5, and even when the disorder range reaches maximum value, 2, the scaling exponent is strictly higher than 0.5, the classical random walker's position distribution scaling exponent.

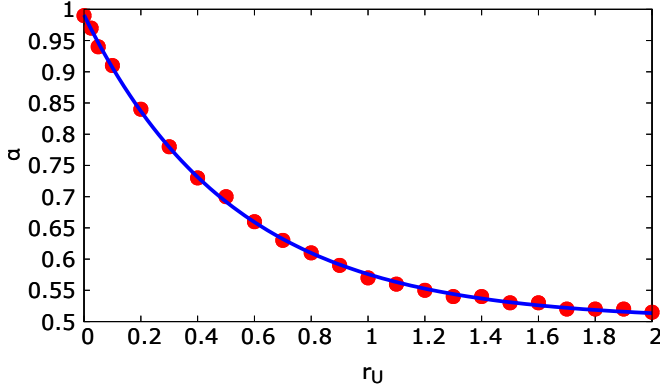


FIG. 6: Response of spread of quantum walker to uniform disorder. We present here the behavior of the scaling exponent of quenched averaged dispersion - as quantified by the quenched averaged standard deviation - of the quantum walker in presence of the uniform quenched disorder in the coin operator. We plot the scaling exponent (α) against the strength, r_U of the uniform disorder applied. The dots represent the values of r_U where a numerical analysis is performed, and the corresponding scaling exponent is explicitly found. The joining curve is the fitted curve, via the method of least squares. See text for further details. All quantities used are dimensionless.

C. Spherical normal disorder

We now analyze the response of the scaling exponent to the disorder that follows the von Mises - Fisher distribution. The profile of α against the disorder strength quantifier, r_N , is exhibited in Figs. 7 and 8. For weak disorder, there is a crossover from a concave to a convex function. This is depicted in Fig. 8, while a general view for a large range of r_N is presented in Fig. 7. We observe that unlike for uniform disorder, for which a $e^{-(\cdot)}$ fit was necessary, the spherical normal distribution would require a $e^{-(\cdot)^2}$ fit, for the scaling exponent against the disorder strength.

From Fig 7, it can be seen that the scaling exponent of the quantum walk decreases with r_N up to a certain value, after which it becomes almost a constant. For large r_N , the exponent converges to a value that is higher than the same in the classical case, and also a little higher than that for large uniform disorder.

The full range of the data, which is presented in Fig. 7, can be fitted with

$$\alpha = a_N \exp(-b_N r_N^2) + c_N, \quad (6)$$

for $a_N = 0.416 \pm 0.00247$, $b_N = 4.81 \pm 0.0768$, and $c_N = 0.578 \pm 0.00134$. The least-square fitting error is 0.00379. The profile of the scaling, as a function of the disorder strength, changes its curvature from being concave to convex, for a relatively low value of the disorder strength, r_N . To exhibit this feature, we plot the same curve as in Fig. 7, again in Fig. 8, but for low values of r_N .

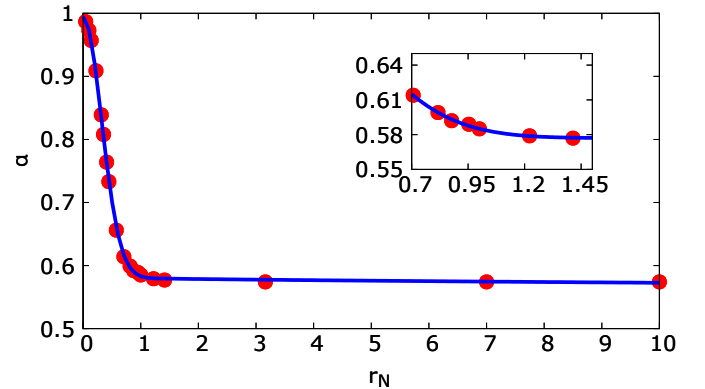


FIG. 7: Scaling behavior in presence of spherical normal disorder. We plot the range of the von Mises - Fisher distribution, r_N , along the horizontal axis and the corresponding value of scaling, α , along the vertical axis. The dots represent the numerical values obtained, while the line is the fitted curve. The inset zooms in on the region where the curve takes a sharp turn. All quantities used are dimensionless.

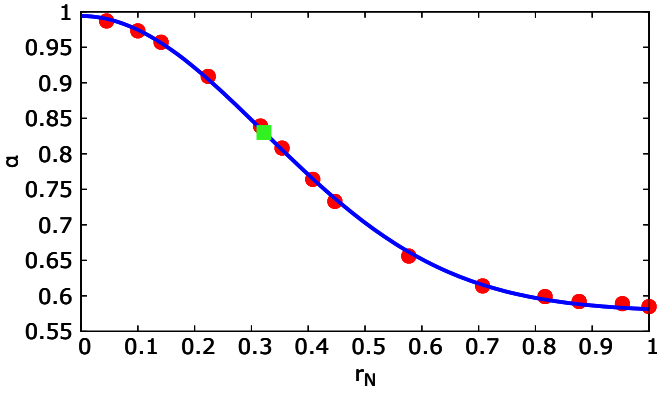


FIG. 8: Scaling of quantum walker's position in presence of weak spherical normal disorder. All considerations are the same as in Fig. 7, except that the disorder strength is weak in the current case, which means that we are zooming in at the region with low r_N values. The point where the profile changes its behavior from being concave to convex, is marked with a green square. It is at $r_N \approx 0.322$.

D. Circular disorder

When the disorder present in the coin operator of quantum walk follows the circular distribution, then the scaling of the DQW varies with the range r_C of the distribution as in Fig. 9, and the fitting function is

$$\alpha = a_C \exp(-b_C r_C^2) + c_C, \quad (7)$$

where $a_C = 0.604 \pm 0.00618$, $b_C = 1.56 \pm 0.0337$, and $c_C = 0.389 \pm 0.00679$. The corresponding error is $= 0.00204$. Like for the vMF distribution and unlike the uniform distribution, the scaling exponent is concave for weak disorder, which then switches to a convex behavior for higher values of the disorder strength. The point from where it switches to convex from concave is approximately $= 0.602$. This point is denoted by a green square in Fig. 9. However, like both the previous types of disorder, the scaling exponent stops a little higher than the classical value (of 0.5), for high disorder strength.

E. Spherical Cauchy-Lorentz disorder

1. Cauchy-Lorentz I

The scaling of quenched averaged dispersion of the quantum walk, with respect to the strength of the disorder distributed as Cauchy-Lorentz I is presented in Fig. 10. The data can be fitted with

$$\alpha = a_1 \exp(-b_1 r_{C1}) + c_1 r_{C1}^{d_1} + e_1 \quad (8)$$

where $a_1 = 0.238 \pm 0.0119$, $b_1 = 9.36 \pm 1.36$, $c_1 = 0.00109 \pm 0.00386$, $d_1 = 2.55 \pm 2.53$ and $e_1 = 0.578 \pm 0.00771$. The corresponding least squares fitting error is 0.0125.

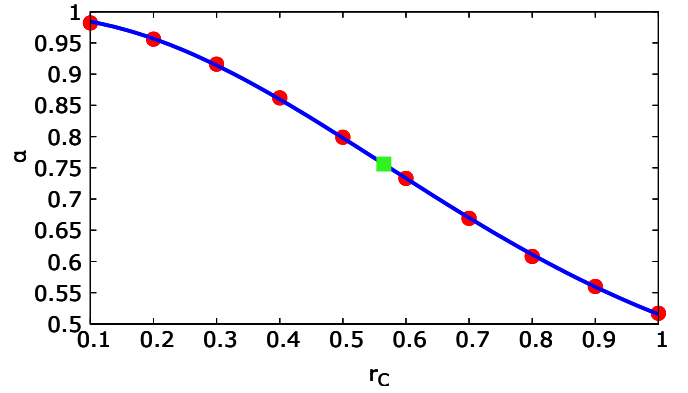


FIG. 9: How does circular disorder present in coin affect the motion of a quantum walker? The considerations are the same as in the preceding three figures, except that the disorder inflicted is from the circular distribution, and the horizontal axis represents the circular disorder strength, r_C . The green square indicates the transition of the curve from concave to convex behavior. See text for more details. All quantities used are dimensionless.

The scaling exponent of the disorder-averaged standard deviation of the walker's position distribution is minimal near $r_{C1} = 1$. Note that $r_{C1} = 1$ corresponds to the Cauchy-Lorentz I distribution with the maximal standard deviation among the distributions with varying δ .

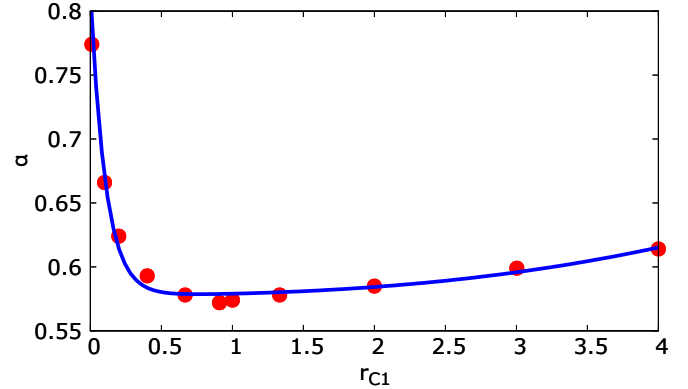


FIG. 10: Illustration of scaling in presence of Cauchy-Lorentz I disorder in DQRW. The considerations are the same as in the preceding few figures, except that the disorder distribution is Cauchy-Lorentz I, and the horizontal axis represents the strength of that disorder. All quantities used are dimensionless.

2. Cauchy-Lorentz II

We now calculate the α in presence of Cauchy-Lorentz II disorder in the quantum coin. The results are presented in Fig. 11, in an α versus disorder strength plot. We fit the data

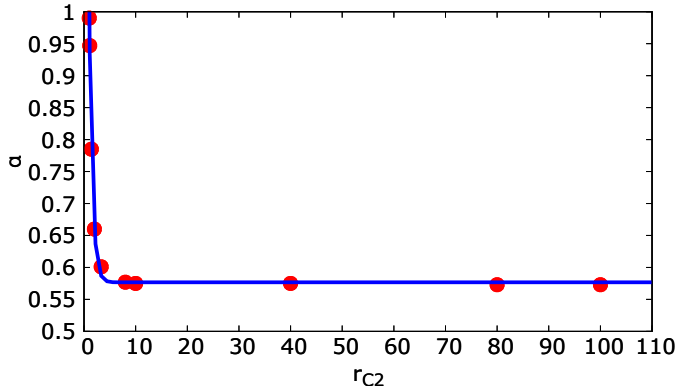


FIG. 11: Scaling behavior of dispersion due to disordered quantum coin following the Cauchy-Lorentz II distribution. The considerations are the same as in the preceding few figures, except that the disorder distribution is Cauchy-Lorentz II, and the horizontal axis is for the strength of that disorder. All quantities used are dimensionless.

with the relation,

$$\alpha = a_2 \exp(-b_2 r_{C2}) + c_2. \quad (9)$$

where $a_2 = 2.13 \pm 0.188$, $b_2 = 1.60 \pm 0.0810$ and $c_2 = 0.577 \pm 0.00353$. The corresponding least squares error is 0.00841. The low disorder limit is similar to the uniform, i.e., the scaling exponent swiftly falls to a near-classical value without a transition from concave to convex. For high disorder, the exponent is near but higher than the classical value of 0.5.

VI. CONCLUSION

In a real experiment, it is almost impossible to completely remove the presence of disorder in system parameters. Fur-

thermore, disorder often induces advantages in system characteristics and resource efficiencies over the ordered case, and may uncover interesting phases of a system. It is therefore interesting to consider the response to disorder in system parameters of a quantum device and its advantage over the classical parallels. It is also interesting to note that disorder can now be artificially incorporated in physical systems realized in the laboratories.

In this work, we analyzed the response of the spread of a quantum walker when the coin operation of the device's set-up is affected by glassy (or quenched) disorder, that is, a type of disorder in which the equilibration time of the disorder is several orders of magnitude higher than the typical observation times that we are interested in. We considered several paradigmatic disorder distributions on the sphere, to consider disorder insertion in the quantum coin's "disordered Hadamard operation". We investigated in particular the scaling exponent of the quenched averaged spread of the quantum walker's position, as quantified by the standard deviation of the walker's position distribution. We found that the scaling exponent is such that the spread in the disordered case, for the distributions considered, is reduced from the ballistic spread in the ordered quantum case. However, the spread remains higher than the dispersive spread of the classical random walker. While this sub-ballistic yet super-dispersive spread is universal for all the distributions of disorder considered, there are significant differences between the behaviors of the scaling exponents of different distributions. In particular, while some disorder distributions lead to slow, Gaussian-like reductions - with increasing disorder strength - of the scaling exponent of the spread, for others, the decay is exponential.

ACKNOWLEDGMENTS

We acknowledge partial support from the Department of Science and Technology, Government of India through the QuEST grant (grant number DST/ICPS/QUEST/Theme-3/2019/120).

[1] R. Feynman, Space-time approach to non-relativistic quantum mechanics, *Rev. Mod. Phys.* **20**, 367 (1948).

[2] Y. Aharonov, L. Davidovich, and N. Zagury, Quantum random walks, *Phys. Rev. A* **48**, 1687 (1993).

[3] A. Nayak and A. Vishwanath, Quantum walk on the line, [arXiv:quant-ph/0010117](https://arxiv.org/abs/quant-ph/0010117).

[4] A. Ambainis, E. Bach, A. Nayak, A. Vishwanath, and J. Watrous, One-dimensional quantum walks, *Proceedings of STOC'01*, pp. 37-49.

[5] J. Kempe, Quantum random walks - an introductory overview, *Contemp. Phys.* **44**, 307 (2003).

[6] V. Kendon, Decoherence in quantum walks - a review, *Math. Struct. in Comp. Sci.* **17**, 1169 (2006).

[7] T. Kitagawa, Topological phenomena in quantum walks; elementary introduction to the physics of topological phases, [arXiv:1112.1882](https://arxiv.org/abs/1112.1882).

[8] O. Mülken and A. Blumen, Continuous-time quantum walks: models for coherent transport on complex networks, *Phys. Rep.* **502**, 37 (2011).

[9] T. Kitagawa, Topological phenomena in quantum walks: elementary introduction to the physics of topological phases, *Quantum Inf. Process.* **11**, 1107 (2012).

[10] S. E. Venegas-Andraca, Quantum walks: a comprehensive review, *Quantum Inf. Process.* **11**, 1015 (2012).

[11] Y. Shikano, From discrete time quantum walk to continuous time quantum walk in limit distribution, *J. Comput. Theor. Nanosci.* **10**, 1558 (2013).

[12] F. Xia, J. Liu, H. Nie, Y. Fu, L. Wan, and X. Kong, Random walks: A review of algorithms and applications, *IEEE Transactions on Emerging Topics in Computational Intelligence*, **4**, 95 (2020).

[13] B. C. Travaglione and G. J. Milburn, Implementing the quantum random walk, *Phys. Rev. A* **65**, 032310 (2002).

[14] A. M. Childs, R. Cleve, E. Deotto, E. Farhi, S. Gutmann, and

D. A. Spielman, Exponential algorithmic speedup by quantum walk, Proc. 35th ACM Symposium on Theory of Computing (STOC 2003), pp. 59-68.

[15] W. Dai, n-Qubit operations on sphere and queueing scaling limits for programmable quantum computer, arXiv:2109.14266.

[16] S. Akmal and C. Jin, Near-optimal quantum algorithms for string problems, arXiv:2110.09696.

[17] C. M. Chandrashekhar and T. Busch, Localized quantum walks as secured quantum memory, *Europhys. Lett.* **110**, 10005 (2015).

[18] R. Asaka, K. Sakai, and R. Yahagi, Quantum random access memory via quantum walk, *Quantum Sci. Technol.* **6**, 035004 (2021).

[19] D. Aharonov, A. Ambainis, J. Kempe, and U. Vazirani, Quantum walks on graphs, arXiv:quant-ph/0012090.

[20] A. M. Childs, E. Farhi, and S. Gutmann, An example of the difference between quantum and classical random walks, *Quantum Inf. Processing* **1**, 35 (2002).

[21] P. Kurzyński and A. Wójcik, Discrete-time quantum walk approach to state transfer, *Phys. Rev. A* **83**, 062315 (2011).

[22] X. Zhan, H. Qin, Z.-h. Bian, J. Li, and P. Xue, Perfect state transfer and efficient quantum routing: a discrete-time quantum walk approach, *Phys. Rev. A* **90**, 012331 (2014).

[23] İ. Yalçinkaya and Z. Gedik, Qubit state transfer via discrete-time quantum walks, *J. Phys. A: Math. Theor.* **48**, 225302 (2015).

[24] H. Li, J. Li, and X. Chen, Discrete-time quantum walk approach to high-dimensional quantum state transfer and quantum routing, arXiv:2108.04923.

[25] M. Annabestani, M. Hassani, D. Tamascelli, and M. G. A. Paris, Multi-parameter quantum metrology with discrete-time quantum walks, arXiv:2110.02032.

[26] J. Mulherkar, R. Rajdeepak, and V. Sunitha, Quantum simulation of perfect state transfer on weighted cubelike graphs, arXiv:2111.00226.

[27] C. A. Ryan, M. Laforest, J. C. Boileau, and R. Laflamme, Experimental implementation of a discrete-time quantum random walk on an NMR quantum-information processor, *Phys. Rev. A* **72**, 062317 (2005).

[28] H. B. Perets, Y. Lahini, F. Pozzi, M. Sorel, R. Morandotti, and Y. Silberberg, Realization of quantum walks with negligible decoherence in waveguide lattices, *Phys. Rev. Lett.* **100**, 170506 (2008).

[29] M. Karski, L. Frster, J. M. Choi, A. Steffen, W. Alt, D. Meschede, and A. Widera, Quantum walk in position space with single optically trapped atoms, *Science* **325**, 174 (2009).

[30] O. Boada, L. Novo, F. Sciarrino, and Y. Omar, Quantum walks in synthetic gauge fields with three-dimensional integrated photonics, *Phys. Rev. A* **95**, 013830 (2017).

[31] Q.-Q. Wang, X.-Y. Xu, W.-W. Pan, K. Sun, J.-S. Xu, G. Chen, Y.-J. Han, C.-F. Li, and G.-C. Guo, Dynamic-disorder-induced enhancement of entanglement in photonic quantum walks, *Optica* **5**, 1136 (2018).

[32] D. T. Nguyen, T. A. Nguyen, R. Khrapko, D. A. Nolan, and N. F. Borrelli, Quantum Walks in periodic and quasiperiodic Fibonacci fibers, arXiv:1911.01389.

[33] M. Gong, S. Wang, and C. Zha, Quantum walks on a programmable two-dimensional 62-qubit superconducting processor, *Science* **372**, 948 (2021).

[34] O. L. Acevedo and T. Gobron, Quantum walks on Cayley graphs, *J. Phys. A: Math. Gen.* **39**, 585 (2006).

[35] G. Leung, P. Knott, J. Bailey, and V. Kendon, Coined quantum walks on percolation graphs, *New J. Phys.* **12**, 123018 (2010).

[36] R. Portugal, R. A. M. Santos, T. D. Fernandes, and D. N. Gonçalves, The staggered quantum walk model, *Quantum Inf. Processing* **15**, 85 (2016).

[37] J. Jayakumar, S. Das, A. Sen(De), and U. Sen, Interference-induced localization in quantum random walk on clean cyclic graph, *EPL* **128**, 20007 (2019).

[38] M. Kieferova and D. Nagaj, Quantum walks on necklaces and mixing, *International Journal of Quantum Information* **10**, 1250025 (2012).

[39] S. R. Jackson, T. J. Khoo, and F. W. Strauch, Quantum walks on trees with disorder: decay, diffusion, and localization, *Phys. Rev. A* **86**, 022335 (2012).

[40] C. Benedetti, M. A. C. Rossi, and M. G. A. Paris, Continuous-time quantum walks on dynamical percolation graphs, *EPL* **124**, 60001 (2018).

[41] P. Sin and J. Sorci, Continuous-time quantum walks on Cayley graphs of extraspecial groups, arXiv:2011.07566.

[42] M. S. Rudner and L. S. Levitov, Topological transition in a non-Hermitian quantum walk, *Phys. Rev. Lett.* **102**, 065703 (2009).

[43] T. Kitagawa, M. S. Rudner, E. Berg, and E. Demler, Exploring topological phases with quantum walks, *Phys. Rev. A* **82**, 033429 (2010).

[44] D. Bagrets, K. W. Kim, S. Barkhofen, S. De, J. Sperling, C. Silberhorn, A. Altland, and T. Micklitz, Probing the topological Anderson transition with quantum walks, *Phys. Rev. Research* **3**, 023183 (2021).

[45] S. Barkhofen, T. Nitsche, F. Elster, L. Lorz, A. Gábris, I. Jex, and C. Silberhorn, Measuring topological invariants in disordered discrete-time quantum walks, *Phys. Rev. A* **96**, 033846 (2017).

[46] X. Zhan, L. Xiao, Z. Bian, K. Wang, X. Qiu, B. C. Sanders, W. Yi, and P. Xue, Detecting topological invariants in nonunitary discrete-time quantum walks, *Phys. Rev. Lett.* **119**, 130501 (2017).

[47] T. Rakovszky, J. K. Asbóth, and A. Alberti, Detecting topological invariants in chiral symmetric insulators via losses, *Phys. Rev. B* **95**, 201407(R) (2017).

[48] F. Cardano, A. D'Errico, A. Dauphin, M. Maffei, B. Piccirillo, C. de Lisio, G. De Filippis, V. Cataudella, E. Santamato, L. Marrucci, M. Lewenstein, and P. Massignan, Detection of zak phases and topological invariants in a chiral quantum walk of twisted photons, *Nature Comm.* **8**, 15516 (2017).

[49] D. Xie, T.-S. Deng, T. Xiao, W. Gou, T. Chen, W. Yi, and B. Yan, Topological quantum walks in momentum space with a Bose-Einstein condensate, *Phys. Rev. Lett.* **124**, 050502 (2020).

[50] A. Schreiber, K. N. Cassemiro, V. Potoček, A. Gábris, I. Jex, and Ch. Silberhorn, Decoherence and disorder in quantum walks: from ballistic spread to localization, *Phys. Rev. Lett.* **106**, 180403 (2011).

[51] H. Lavička, V. Potoček, T. Kiss, E. Lutz, and I. Jex, Quantum walk with jumps, *Eur. Phys. J. D* **64**, 119 (2011).

[52] J. Svozilsk, R. de J. León-Montiel, and J. P. Torres, Implementation of a spatial two-dimensional quantum random walk with tunable decoherence, *Phys. Rev. A* **86**, 052327 (2012).

[53] M. A. Pires and S. M. D. Queirós, Quantum walks with sequential aperiodic jumps, *Phys. Rev. E* **102**, 012104 (2020).

[54] T. Oka, N. Konno, R. Arita, and H. Aoki, Breakdown of an electric-field driven system: a mapping to a quantum walk, *Phys. Rev. Lett.* **94**, 100602 (2005).

[55] R. J. Sension and R. J. Sension, Quantum path to photosynthesis, *Nature (London)* **446**, 740 (2007).

[56] M. Mohseni, P. Rebentrost, S. Lloyd, and A. Aspuru-Guzik,

Environment-assisted quantum walks in photosynthetic energy Transfer, *J. of Chem. Phys.* **129**, 174106 (2008).

[57] A. Aharony, Spin-flop multicritical points in systems with random fields and in spin glasses, *Phys. Rev. B* **18**, 3328 (1978).

[58] G. Misguich and C. Lhuillier, Two-dimensional quantum antiferromagnets, in frustrated spin systems, edited by H. T. Diep (World-Scientific, Singapore, 2005).

[59] J. Villain, R. Bidaux, J.-P. Carton, and R. Conte, Order as an effect of disorder, *J. Physique* **41**, 1263 (1980); B. J. Minchau and R. A. Pelcovits, Two-dimensional XY model in a random uniaxial field, *Phys. Rev. B* **32**, 3081 (1985); C. L. Henley, Ordering due to disorder in a frustrated vector antiferromagnet, *Phys. Rev. Lett.* **62**, 2056 (1989); A. Moreo, E. Dagotto, T. Jolicoeur, and J. Riera, Cu^{63} Knight shifts in the superconducting state of $YBa_2Cu_3O_{7-\delta}$ ($T_c=90$ K), *Phys. Rev. B* **42**, 6283 (1990); D. E. Feldman, Exact zero-temperature critical behaviour of the ferromagnet in the uniaxial random field, *J. Phys. A* **31**, L177 (1998); G. E. Volovik, Random anisotropy disorder in superfluid 3He -A in aerogel, *JETP Lett.* **84**, 455 (2006); D. A. Abanin, P. A. Lee, and L. S. Levitov, Randomness-induced XY ordering in a graphene quantum hall ferromagnet, *Phys. Rev. Lett.* **98**, 156801 (2007); L. Adamska, M. B. Silva Neto, and C. Morais Smith, $La_{2-x}Sr_xCu_{1-z}Zn_zO_4$: Role of Dzyaloshinskii-Moriya and XY anisotropies, *Phys. Rev. B* **75**, 134507 (2007);

[60] L. F. Santos, G. Rigolin, and C. O. Escobar, Entanglement versus chaos in disordered spin chains, *Phys. Rev. A* **69**, 042304 (2004); C. Mejía-Monasterio, G. Benenti, G. G. Carlo, and G. Casati, Entanglement across a transition to quantum chaos, *Phys. Rev. A* **71**, 062324 (2005); A. Lakshminarayanan and V. Subrahmanyam, Multipartite entanglement in a one-dimensional time-dependent Ising model, *Phys. Rev. A* **71**, 062334 (2005); J. Karthik, A. Sharma, and A. Lakshminarayanan, Entanglement, avoided crossings, and quantum chaos in an Ising model with a tilted magnetic field, *Phys. Rev. A* **75**, 022304 (2007); W. G. Brown, L. F. Santos, D. J. Sterling, and L. Viola, Quantum chaos, delocalization, and entanglement in disordered heisenberg models, *Phys. Rev. E* **77**, 021106 (2008); F. Dukesz, M. Zilbergerts, and L. F. Santos, Interplay between interaction and (un)correlated disorder in one-dimensional many-particle systems: delocalization and global entanglement, *New J. Phys.* **11**, 043026 (2009); J. Hide, W. Son, and V. Vedral, Enhancing the detection of natural thermal entanglement with disorder, *Phys. Rev. Lett.* **102**, 100503 (2009); K. Fujii and K. Yamamoto, Anti-Zeno effect for quantum transport in disordered systems, *Phys. Rev. A* **82**, 042109 (2010).

[61] R. Prabhu, S. Pradhan, A. Sen(De), and U. Sen, Disorder overtakes order in information concentration over quantum networks, *Phys. Rev. A* **84**, 042334 (2011).

[62] P. V. Martín, J. A. Bonachela, and M. A. Muñoz, Quenched disorder forbids discontinuous transitions in nonequilibrium low-dimensional systems, *Phys. Rev. E* **89**, 012145 (2014).

[63] A. Niederberger, T. Schulte, J. Wehr, M. Lewenstein, L. Sanchez-Palencia, and K. Sacha, Disorder-induced order in two-component Bose-Einstein condensates, *Phys. Rev. Lett.* **100**, 030403 (2008); A. Niederberger, J. Wehr, M. Lewenstein, and K. Sacha, Disorder-induced phase control in superfluid Fermi-Bose mixtures, *Europhys. Letts.* **86**, 26004 (2009); A. Niederberger, M. M. Rams, J. Dziarmaga, F. M. Cucchietti, J. Wehr, and M. Lewenstein, Disorder-induced order in quantum XY chains, *Phys. Rev. A* **82**, 013630 (2010); D. I. Tsomokos, T. J. Osborne, and C. Castelnovo, Interplay of topological order and spin glassiness in the toric code under random mag-

netic fields, *Phys. Rev. B* **83**, 075124 (2011); M. S. Foster, H.-Y. Xie, and Y.-Z. Chou, Topological protection, disorder, and interactions: survival at the surface of three-dimensional topological superconductors, *Phys. Rev. B* **89**, 155140 (2014).

[64] P. Ribeiro, P. Milman, and R. Mosseri, Aperiodic quantum random walks, *Phys. Rev. Lett.* **93**, 190503 (2004).

[65] M. C. Bañuls, C. Navarrete, A. Pérez, E. Roldán, and J. C. Sóriano, Quantum walk with a time-dependent coin, *Phys. Rev. A* **73**, 062304 (2006).

[66] D. Bulger, J. Freckleton, and J. Twamley, Position-dependent and cooperative quantum Parrondo walks, *New J. Phys.* **10**, 093014 (2008).

[67] A. Romanelli, The fibonacci quantum walk and its classical trace map, *Physica A* **388**, 3985 (2009).

[68] A. Romanelli, Driving quantum-walk spreading with the coin operator, *Phys. Rev. A* **80**, 042332 (2009).

[69] Y. Shikano and H. Katsura, Localization and fractality in inhomogeneous quantum walks with self-duality, *Phys. Rev. E* **82**, 031122 (2010).

[70] C. M. Chandrashekar, Disordered-quantum-walk-induced localization of a Bose-Einstein condensate, *Phys. Rev. A* **83**, 022320 (2011).

[71] C. Ampadu, Limit Theorems for the Disordered quantum Walk, arXiv:1108.6110.

[72] A. Ahlbrecht, V. B. Scholz, and A. H. Werner, disordered quantum walks in one lattice dimension, *J. Math. Phys.* **52**, 102201 (2011).

[73] C. M. Chandrashekar, Disordered quantum walk-induced localization of a Bose-Einstein condensate, *Phys. Rev. A* **83**, 022320 (2011).

[74] A. Ahlbrecht, C. Cedzich, R. Matjeschk, V. B. Scholz, A. H. Werner, and R. F. Werner, Asymptotic behavior of quantum walks with spatio-temporal coin fluctuations, *Quantum Inf. Processing* **11**, 1219 (2012).

[75] C. M. Chandrashekar, Disorder induced localization and enhancement of entanglement in one- and two-dimensional quantum walks, arXiv:1212.5984.

[76] R. Vieira, E. P. M. Amorim, and G. Rigolin, Dynamically disordered quantum walk as a maximal entanglement generator, *Phys. Rev. Lett.* **111**, 180503 (2013).

[77] N. Konno, T. Łuczak, and E. Segawa, Limit measures of inhomogeneous discrete-time quantum walks in one dimension, *Quantum Inf. Processing* **12**, 33 (2013).

[78] R. Zhang, P. Xue, and J. Twamley, One-dimensional quantum walks with single-point phase defects, *Phys. Rev. A* **89**, 042317 (2014).

[79] R. Vieira, E. P. M. Amorim, and G. Rigolin, Entangling power of disordered quantum walks, *Phys. Rev. A* **89**, 042307 (2014).

[80] B. Tarasinski, J. K. Asbóth, and J. P. Dahlhaus, Scattering theory of topological phases in discrete-time quantum walks, *Phys. Rev. A* **89**, 042327 (2014).

[81] C. M. Chandrashekar and T. Busch, Quantum percolation and transition point of a directed discrete-time quantum walk, *Sci. Rep.* **4**, 6583 (2014).

[82] M. Montero, Invariance in quantum walks with time-dependent coin operators, *Phys. Rev. A* **90**, 062312 (2014).

[83] Q. Zhao and J. Gong, From disordered quantum walk to physics of off-diagonal disorder, *Phys. Rev. B* **92**, 214205 (2015).

[84] T. Rakovszky and J. K. Asbóth, Localization, delocalization, and topological phase transitions in the one-dimensional split-step quantum walk, *Phys. Rev. A* **92**, 052311 (2015).

[85] M. Montero, Classical-like behavior in quantum walks with inhomogeneous, time-dependent coin operators, *Phys. Rev. A*

93, 062316 (2016).

[86] S. Chakraborty, A. Das, A. Mallick, and C. M. Chandrashekar, Quantum ratchet in disordered quantum walk, *Annalen der Physik*, **529**, 8, 1600346 (2017).

[87] K. Mochizuki, H. Obuse, Effects of disorder on non-unitary \mathcal{PT} symmetric quantum walks, *Interdisciplinary Information Sciences* **23**, 95 (2017).

[88] A. D. Verga, Edge states in a two-dimensional quantum walk with disorder, *Eur. Phys. J. B* **90**, 41 (2017).

[89] S. Singh and C. M. Chandrashekar, Quantum interference and coherence in one-dimensional disordered and localized quantum walk, arXiv:1711.06217.

[90] N. P. Kumar, S. Banerjee, and C. M. Chandrashekar, Enhanced non-markovian behavior in quantum walks with markovian disorder, *Sci. Rep.* **8**, 8801 (2018).

[91] G. D. Molfetta, D. O. Soares-Pinto, and S. M. D. Queirós, Elephant quantum walk, *Phys. Rev. A* **97**, 062112 (2018).

[92] A. C. Orthey Jr. and E. P. M. Amorim, Weak disorder enhancing the production of entanglement in quantum walks, *Braz. J. Phys.* **49**, 595 (2019).

[93] S. Das, S. Mal, A. Sen, and U. Sen, Inhibition of spreading in quantum random walks due to quenched Poisson-distributed disorder, *Phys. Rev. A* **99**, 042329 (2019).

[94] M. A. Pires and S. M. D. Queirós, Negative correlations can play a positive role in disordered quantum walks, arXiv:2008.08867.

[95] M. A. Pires and S. M. D. Queirós, Genuine Parrondo's paradox in quantum walks with time-dependent coin operators, *Phys. Rev. E* **102**, 042124 (2020).

[96] P. Sen, Scaling and crossover behaviour in a truncated long range quantum walk, *Physica A* **545**, 123529 (2020).

[97] F. Nosrati, A. Laneve, M. K. Shadfar, A. Gerald, K. Mavadipour, F. Pegoraro, P. Mataloni, and R. L. Franco, Quantum information spreading in a disordered quantum walk, *J. Opt. Soc. Am. B* **38**, 2570 (2021).

[98] D. Bagrets, K. W. Kim, S. Barkhofen, S. De, J. Sperling, C. Silberhorn, A. Altland, and T. Micklitz, Probing the topological anderson transition with quantum walks, *Phys. Rev. Research* **3**, 023183 (2021).

[99] M. Kac, Random walk and the theory of Brownian motion, *The American Mathematical Monthly*, **54**, 369 (1947).

[100] F. B. Knight, On the random walk and Brownian motion, *Trans. Amer. Math. Soc.* **103**, 218 (1962).

[101] J. Åberg, Quantifying superposition, arXiv:quant-ph/0612146.

[102] T. Baumgratz, M. Cramer, and M. B. Plenio, Quantifying coherence, *Phys. Rev. Lett.* **113**, 140401 (2014).

[103] A. Winter and D. Yang, Operational resource theory of coherence, *Phys. Rev. Lett.* **116**, 120404 (2016).

[104] A. Streltsov, G. Adesso, and M. B. Plenio, Quantum coherence as a resource, *Rev. Mod. Phys.* **89**, 041003 (2017).

[105] T. Theurer, N. Killoran, D. Egloff, and M. B. Plenio, Resource theory of superposition, *Phys. Rev. Lett.* **119**, 230401 (2017); S. Das, C. Mukhopadhyay, S. S. Roy, S. Bhattacharya, A. Sen(De), and U. Sen, Wave-particle duality employing quantum coherence in superposition with non-orthogonal pointers, *J. Phys. A: Math. Theor.* **53**, 115301 (2020).

[106] C. Srivastava, S. Das, and U. Sen, Resource theory of quantum coherence with probabilistically nondistinguishable pointers and corresponding wave-particle duality, *Phys. Rev. A* **103**, 022417 (2021).

[107] I. Banerjee, K. Sen, C. Srivastava, and U. Sen, Quantum coherence with incomplete set of pointers and corresponding wave-particle duality, arXiv:2108.05849.

[108] M. B. Plenio and S. Virmani, An introduction to entanglement measures, *Quant. Inf. Comput.* **7**, 1 (2007).

[109] R. Horodecki, P. Horodecki, M. Horodecki, and K. Horodecki, Quantum entanglement, *Rev. Mod. Phys.* **81**, 865 (2009).

[110] O. Gühne and G. Tóth, Entanglement detection, *Physics Reports* **474**, 1 (2009).

[111] S. Das, T. Chanda, M. Lewenstein, A. Sanpera, A. Sen(De), and U. Sen, The separability versus entanglement problem, in *Quantum Information*, edited by D. Bruß and G. Leuchs (Wiley, Weinheim, 2019), chapter 8.

[112] R. M. Clark and B. J. Morrison, A normal approximation to the Fisher distribution, *Geophys. J. R. Astr. Soc.* **13**, 271 (1983).

[113] T. D. Downs, Cauchy families of directional distributions closed under location and scale transformations, *The Open Statistics & Probability Journal*, **1**, 76 (2009).

[114] S. Kato and P. McCullagh, Möbius transformation and a Cauchy family on the sphere, *Bernoulli*, **26**, 3224 (2020).